HZP and HFP rod ejection analysis in a SMART-like reactor model using the GUARDYAN-SUBCHANFLOW coupled code system

Előd Pázmán [a],[*], Gábor Tolnai [a], Dávid Légrády [a], Luigi Mercatali [b], Gianfranco Huaccho [b], Victor Hugo Sanchez-Espinoza [b]

[a] Department of Nuclear Techniques, Institute of Nuclear Techniques, Budapest University of Technology and Economics, Műegyetem rkp. 3., Budapest, 1111, Hungary
[b] Karlsruhe Institute of Technology, Institute for Neutron Physics and Reactor Technology, Hermann-von-Helmholtz-Platz 1, Eggenstein-Leopoldshafen, 76344, Germany

ABSTRACT

GUARDYAN is a dynamic 3D Monte Carlo reactor physics code with continuous energy handling developed for GPU hardware that has recently been coupled to the SUBCHANFLOW (SCF) subchannel thermal hydraulics solver. In this paper two control rod ejection accident scenarios will be presented in a Small Modular Reactor (SMR) geometry: a transient starting from Hot Zero Power (HZP), and one starting from Hot Full Power (HFP) conditions, both of them using Beginning of Cycle (BOC) material composition. Both the time dependent core-wise data and the node-wise data at certain times calculated by the GUARDYAN-SCF coupled code system exhibit the tendencies expected during such transients, with the thermal hydraulic properties mostly inside their safe limits. Relative variances estimated from 8 independent realisations suggest the results are credible. To further support our findings the HZP results are presented alongside data from PARCS-SCF and Serpent2-SCF calculations provided by Karlsruhe Institute of Technology (KIT), while for the HFP case we were able to compare some of the quantities to PARCS-SCF results.

1. Introduction

SMR concepts are rapidly gaining popularity as a possible option to lower both the initial cost and the construction time of new nuclear power plants. Reactivity insertion transients such as rod ejection accident scenarios are typical design basis accidents that have to be considered during the licensing process of new reactor designs. Traditionally transient safety calculations of this type are done using deterministic (e.g. nodal diffusion) codes exhibiting relatively fast runtimes.

Due to the availability of high performance computing architectures high resolution solutions using Monte Carlo based reactor physics codes are becoming increasingly more affordable even for transient problems. In order to properly model an accident scenario the thermal feedbacks cannot be ignored, thus recently pin-by-pin resolution Monte Carlo neutronics calculations have been coupled with subchannel thermal hydraulics solvers (Legrady et al., 2023; Ferraro et al., 2020) to achieve high fidelity results that previously were not possible.

For novel SMR concepts these high fidelity results can be especially useful, since there is a lack of experimental results and operational experience for these reactor types. The relatively still high computational cost can be justified with the value the results can provide as a reference solution for more lightweight deterministic solvers, as it is debated whether diffusion methods are valid for such small scale high leakage systems. A comparison of deterministic and Monte Carlo solutions of the same problem can be found in a recent study (Mercatali et al., 2023) carried out at Karlsruhe Institute of Technology (KIT) comparing two coupled neutronics-thermal hydraulics code systems, namely Serpent2 (Leppänen et al., 2015) high fidelity Monte Carlo based neutronics and PARCS (Downar, 2017) deterministic nodal diffusion calculations, both coupled with the SUBCHANFLOW (Imke and Sanchez, 2012) subchannel thermal hydraulics solver.

We will build on this paper to further explore the possibilities of high fidelity dynamic Monte Carlo calculations for SMR applications. Using the GUARDYAN code (Legrady et al., 2022) coupled with SUBCHANFLOW we provide an additional Monte Carlo based solution for the HZP problem proposed in Mercatali et al. (2023), as well as a solution for a similar transient starting from HFP initial conditions.

First, we will briefly introduce GUARDYAN and the other codes used for the calculations in Section 2, Section 3 contains the description of the SMR model developed at KIT that was used for the simulations

---

* Corresponding author.
  E-mail address: pazmanelod@reak.bme.hu (E. Pázmán).

with the simulation details and models. The calculation results, along with some error analysis for the GUARDYAN solutions are presented in Section 4 and are summarised in Section 5.

2. The codes used

2.1. GUARDYAN

The GUARDYAN (GPU Assisted Reactor Dynamic Analysis) dynamic Monte Carlo reactor physics code is being developed at the Budapest University of Technology and Economics (BME), Hungary. The code simulates 3D neutron transport with continuous energy handling and direct time dependence, using Graphics Processing Units (GPUs) as hardware.

The model geometry is given by cells of homogeneous material composition built up using Constructive Solid Geometry, i.e.: the cells are bounded by a set of (up to fourth order) surfaces connected by boolean operators. Temperatures and densities can be given separately for each cell by its material or on a superimposed mesh. Cross section data is given in ACE format. Time dependent input is given in separate input files for each time step, or by change in density and/or temperature, or by applying time dependent transformations to parts of the geometry. GUARDYAN uses Woodcock (delta-) tracking for free path sampling, thus time dependent changes can be taken into account on a continuous scale if needed. Reactions are sampled based on their cross sections, and the probability densities of the chosen interaction are sampled according to the corresponding ACE laws to produce the new energy and direction of the neutron.

An even distribution of the workload between GPU threads is needed to fully utilise the hardware. For this, GUARDYAN divides the simulation into time intervals so population control techniques, specifically the combing (Legrady et al., 2020) of particle populations, can be applied both to reduce variance and to have a constant number of live neutrons to keep all threads busy. During the time intervals GUARDYAN simulates transport according to the improved branchless method (Sjenitzer and Hoogenboom, 2013) to eliminate most conditional loops and branching statements from the algorithm, thus reducing the possibilities for significant thread divergence. Vastly different prompt and delayed neutron lifetimes would also introduce stalled threads, this is avoided by sampling the delayed neutron precursor isotopes instead of the delayed neutrons themselves, and applying forced decay at the beginning of time intervals (Legrady and Hoogenboom, 2008). Dynamic GUARDYAN calculations are started from an initial static ($k_{eff=1}$) state, for which a converged source is reached, then a bank of delayed neutron precursor isotopes is filled up from the converged source before the start of the transient itself.

Code-to-code verification of the transport physics in both criticality and fixed-source calculations was carried out for every isotope, consisting of the comparison of about half a million data points and several integral quantities from the ICSBEP (Molnar et al., 2019) benchmark set. Validation of the GUARDYAN code using real life data was done for small scale systems using measurement data of kinetic transients of the BME Training Reactor (Boroczki et al., 2020), and for large scale systems ex-core flux detector data from the 4th unit of Paks nuclear power plant was used (Legrady et al., 2022).

GUARDYAN is coupled with SUBCHANFLOW (Legrady et al., 2023) in a Semi-Implicit Operator-Splitting scheme, where neutronics and thermal-hydraulic calculations are alternated with the power and thermal hydraulics properties taken from the previous step. During the source convergence the pin-node level normalised power data is given to a static SUBCHANFLOW calculation that provides an equilibrium distribution of the fuel temperature, coolant temperature, and coolant density for the next neutronics step. A convergence in the thermal hydraulics properties also has to be reached before precursor generation. During the transient calculation the power is left to evolve, instead of normalisation just a constant scaling factor is applied and this power data is given to a dynamic SUBCHANFLOW calculation with the same timestep as the neutronics. A block diagram of the coupling scheme in the dynamic simulation mode can be seen in Fig. 1.

2.2. SUBCHANFLOW

SUBCHANFLOW is a subchannel thermal-hydraulics code being developed at KIT (Imke and Sanchez, 2012) based on the codes COBRA-IV-I and COBRA-EN. The code solves four conservation equations: mass, enthalpy, and momentum both in axial and transversal direction for single or two-phase upward flow in rod bundles (in rectangular as well as triangular lattices) both in stationary and transient scenarios. Properties of water and steam are calculated according to IAPWS-97 (International Association for the Properties of Water and Steam), but functions for other working fluids like liquid metals and gases are also implemented. Mixing between neighbouring subchannels is calculated as a function of the pressure difference or from a constant mixing factor, turbulent mixing is empirically modelled. Heat conduction in the fuel and cladding is solved based on a finite volume method using temperature dependent thermophysical properties of the materials. Several reactor physics codes (both deterministic and Monte Carlo based) have been coupled with SUBCHANFLOW in the past decade (Legrady et al., 2023; Ferraro et al., 2020; Basualdo et al., 2020; Garcia et al., 2019; Sanchez-Espinoza et al., 2021), mostly for light water reactor calculations.

2.3. PARCS and Serpent2

The transient calculations at KIT were performed using the PARCS deterministic and Serpent2 Monte Carlo neutron transport codes coupled with SUBCHANFLOW for thermal-hydraulic solutions.

PARCS is a 3D deterministic solver (Downar, 2017) for Cartesian or hexagonal geometries capable of both dynamic and static calculations using either the multi group diffusion method or the SP3 transport equations. Here an approach using finite difference method in the x-y directions with nodal expansion for the z direction was used.

Serpent2 is a 3D Monte Carlo based neutron and photon transport code with continuous energy handling developed at VTT Technical Research Centre of Finland since 2004 (Leppänen et al., 2015). This multi purpose code is widely used for full core calculations, group constant production, depletion calculations, and shielding problems among others. Serpent2 has both static and transient capabilities. Dynamic Serpent2 simulations are started from a known critical system as external source calculations with a time step discretisation for population control purposes. Delayed neutrons are treated by precursor sampling with a separate external source, meaning a steady state calculation is needed before the actual transient (external source) simulation in order to produce both the precursor isotope and live neutron sources and the converged power distribution.

Detailed descriptions of the codes can be found elsewhere (Downar, 2017; Leppänen et al., 2015), and brief introductions in the context of the current calculations is given in the paper on the HZP simulations by KIT (Mercatali et al., 2023).

2.4. Code differences

GUARDYAN and Serpent2 are quite similar in the way they handle transient simulations, as described in Sections 2.1 and 2.3, both codes employ delayed neutron precursor tracking with forced decay, start the transient simulation from a critical source, and divide the transient into time intervals for population control. All of these features emerged as best practices in the last 15 or so years of dynamic Monte Carlo (DMC) research, thus almost all Monte Carlo codes with transient capabilities will have implemented them. The differences between the two codes can be found in the exact implementation of these features: Serpent2 is a "traditional" Monte Carlo code that was originally for criticality calculations on CPU hardware with sequential execution, while GUARDYAN was developed as a dynamic code in the first place, specifically for GPU hardware, so unique considerations had to be made in order to exploit the massively parallel architecture. Some notable differences are:
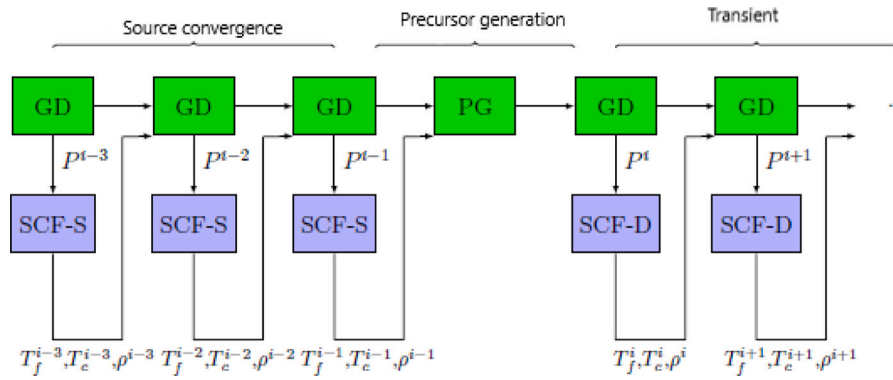
Fig. 1. Coupling scheme between GUARDYAN and SUBCHANFLOW for a dynamic calculation.

- GUARDYAN simulates the neutrons' history in a completely branchless manner, and no splitting and Russian roulette is applied during a time step.
- For the initial source distributions Serpent2 uses separate criticality calculations: during one live neutrons are stored at random times, during the other the delayed neutron precursors are saved. GUARDYAN uses a dynamic calculation with instant precursor decay to reach converged thermal hydraulic and flux distributions, followed by several pure neutronics time steps to bank the delayed neutron precursors at fission sites.
- In transient simulations population control is necessary to keep the number of neutrons low enough to stay inside the memory constraints in a supercritical case, and to keep them from dying out in a subcritical system. In the case of GUARDYAN a constant number of particles is also needed to properly utilise the hardware by balancing the workload between the GPU threads.
- GUARDYAN employs Woodcock tracking exclusively, while Serpent2 uses a combination of Woodcock tracking and surface tracking. As a consequence GUARDYAN models the control rod movement as a continuous function of time instead of updating the geometry at the time boundaries.
- Both codes can receive geometric data given with constructive solid geometry, while Serpent2 can also handle unstructured mesh geometries.

3. KSMR core model and transient scenarios

The KSMR core is a SMART-like SMR model (Alzaben et al., 2019b) that is a boron-free concept: instead of the more traditional soluble-boron, the design uses advanced burnable absorbers (BAs) in order to have sufficient excess reactivity, while also excluding the possibility of a boron dilution accident by design. The light water cooled KSMR model is optimised to have a nominal thermal power of 330 MW loaded with 57 fuel assemblies (FAs), each being a 17 by 17 square lattice with 24 guide tubes, a central instrumentation tube, and 20 or 24 BA rods depending on their position, with regular fuel pins in the rest of the positions. The material of the BAs is a mixture of Al_2O_3 and B_4C, the fuel pins are made of UO_2 with below 5% enrichments and a Zr-4 cladding. For the simulation 53 assemblies have control rods made of B_4C for a fast safety shutdown, Ag-In-Cd for coarse reactivity control, or Ag-In-Cd and stainless steel for fine reactivity control. The control rod configuration with the initial position of the control rod banks for the HZP and HFP cases are shown on Fig. 2. Both cases assume beginning of cycle (BOC) conditions meaning fresh fuel with simple material composition compared to fuel after burnup. The initial thermal power of the reactor is 330 W for the HZP case and 330 MW for the HFP case corresponding to 10^{-4}% and 100% of the nominal power. The ejected CR bank is the one with the highest reactivity worth both in the HZP and HFP cases, highlighted in Fig. 2. The ejection happens in 0.05 s, and the transient is followed up to 3 s.

For the GUARDYAN and Serpent2 calculations realistic 3D pin-by-pin models were developed using the ENDF-B/VII cross section library with 6 delayed neutron precursor isotope groups for the neutronics with subchannel-by-subchannel resolution thermal-hydraulics using 18 by 18 channels for each 17 by 17 fuel assembly.

The Serpent2 calculation used 20 axial layers on the active core length for tallying. The simulation used 10^5 neutrons for the source generation and 10^7 neutrons in 100 batches for the transient. The time binning of the neutronics, the timestep of the thermal hydraulics, and the coupling step were all 0.006 s. Simulation of the total 3 s of the HZP transient took 2.54 days using 20 nodes of 150 Intel Xeon Platinum 8368 CPUs.

Preliminary studies indicated that for a cosine power distribution about 30 nodes would be optimal in balancing spatial detail and statistical variance of the power estimates of a node when using GUARDYAN-SCF, therefore we increased the spatial resolution: the GUARDYAN model tallied the power in 30 axial layers with the same nodalisation for the thermal hydraulics model. The neutronics timesteps for population control were 10^{-5} s while the coupling steps were 0.001 s, and thermal hydraulics data is saved every 0.006 s. The simulation used 524 288 prompt neutrons with 262 144 precursor particles. The maximum number of thermal hydraulics iterations allowed were limited to 50. The calculations were done using a single NVIDIA GeForce RTX 3090 GPU with an Intel Xeon E5-1620 v4 CPU. For the HZP case the total runtime for the 3 s transient was 11.55 days, of which the runtime of SUBCHANFLOW was 7.95 days. The HFP case took 16.94 days with 7.31 days being the runtime of SUBCHANFLOW. It should be noted that SUBCHANFLOW ran on a single CPU thread.

The material map of the GUARDYAN model can be seen in Fig. 3. The Serpent2 model is virtually identical in terms of geometry.

The PARCS model used two-group constants generated from a 2D pin level fuel assembly model by Serpent2, with 3D full core calculations for the radial reflectors. Radially the model has one node per assembly with 27 layers axially from which 20 is for the active length, 3 and 4 is for the bottom and top reflector respectively. The thermal hydraulics model uses the same discretisation using a single channel with a representative rod for each fuel assembly.

4. Results

The most important peak values (e.g. total power, maximum temperatures, minimum DNBR) are summarised in Table 1. The time evolution and distribution of these quantities, as well as the variances of the GUARDYAN-SCF results will be further discussed. First in Section 4.1 the GUARDYAN-SCF HZP results will be compared to the Serpent2-SCF and PARCS-SCF results made available to us by KIT. In Section 4.2 the GUARDYAN-SCF HFP results will be discussed along some PARCS-SCF results from Alzaben et al. (2019a).
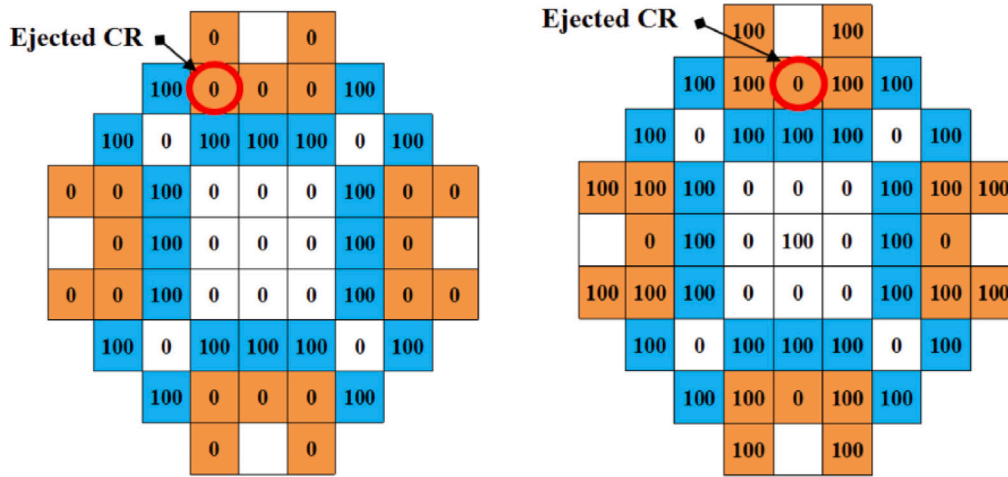
Fig. 2. Control rod configuration of the two cases (left: HZP, right: HFP). Control rod types: blue: B₄C, orange: Ag-In-Cd, white: Ag-In-Cd with stainless steel, initial positions: 0: fully inserted, 100: completely withdrawn.
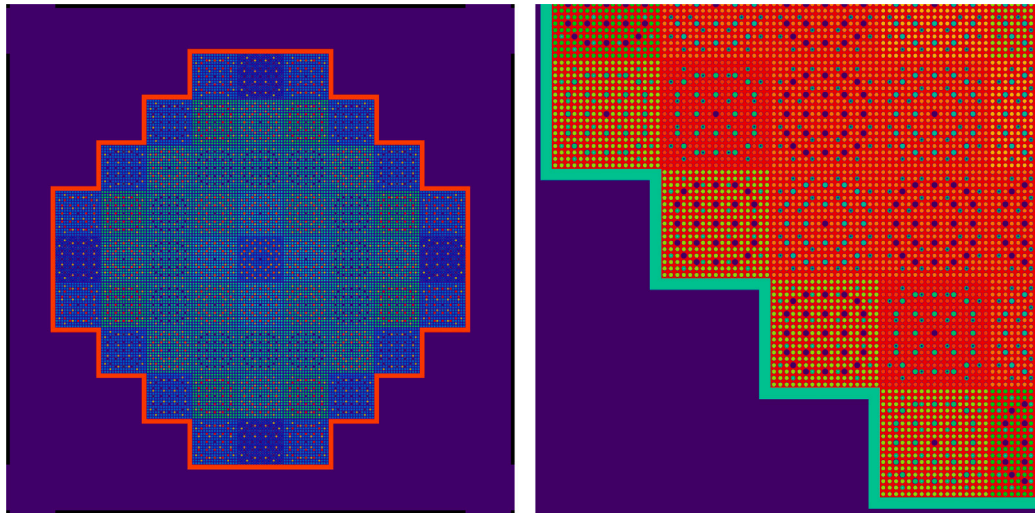

Fig. 3. Material map of the GUARDYAN KSMR model.

Table 1
Peak values and times predicted by the different coupled code systems.

	PARCS-SCF	Serpent2-SCF	GUARDYAN-SCF	
	HZP	HZP	HZP	HFP
Peak power [ratio to nominal]	48.35	36.2	27.8	14.3
Time at peak power [s]	0.1645	0.192–0.198	0.192-0.198	0.066–0.072
Final power [ratio to nominal]	0.23	0.22	0.15	1.18
Minimum DNBR	1.6154	1.3032	1.8538	0.9055
Time at minimum DNBR [s]	0.221	0.246	0.288	0.138
Final MDNBR	4.5304	3.8892	4.8005	1.4051
Max fuel centerline temp [K]	1149	1256	1127	1882
Time at max fuel centerline temp [s]	1.3415	1.53	1.29	2.982
Max coolant temp [K]	605	615	606	615
Time at max coolant temp [s]	1.1545	0.954–1.140	1.128	0.462–0.858
Max cladding inner temp [K]	676	686	672	709
Time at max cladding inner temp [s]	0.2435	0.276	0.276	0.144
Max cladding outer temp [K]	621	622	620	632
Time at max cladding outer temp [s]	0.217	0.258	0.276	0.222

4.1. HZP results

Comparison of the evolution of the total power can be seen in Fig. 4, the time when the ejected control rod is fully out is marked by the dashed red line on all time evolution plots. The power data calculated by GUARDYAN-SCF was averaged over 6 ms intervals to

have the same time resolution as the other quantities. The location of the peak power according to the PARCS-SCF calculation is somewhat earlier, 0.1645 s, than according to the Monte Carlo codes, both of which has the maximum in the same time bin, 1.192 s – 0.198 s. The maximum power estimated by Serpent2-SCF is 36.2 times the nominal power, and 27.8 times according to the GUARDYAN-SCF calculations,
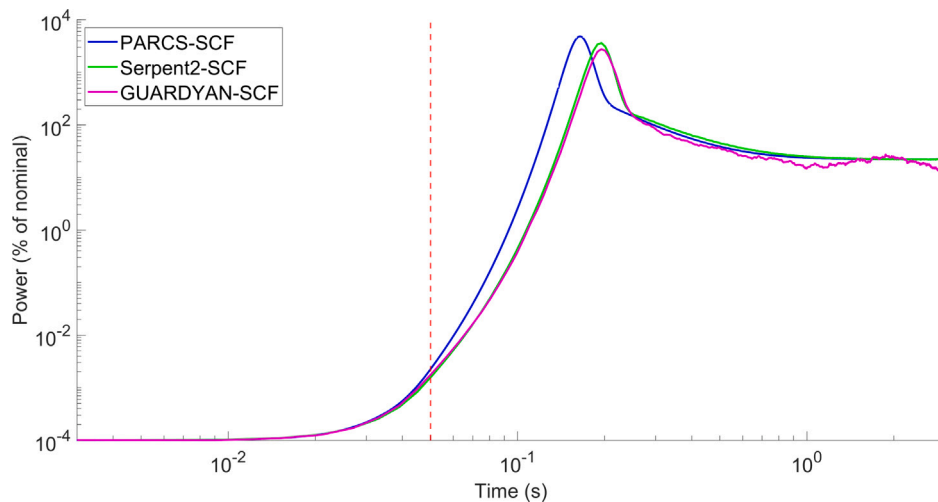
Fig. 4. Evolution of the total power during the transient starting from HZP as calculated by the three different code systems.
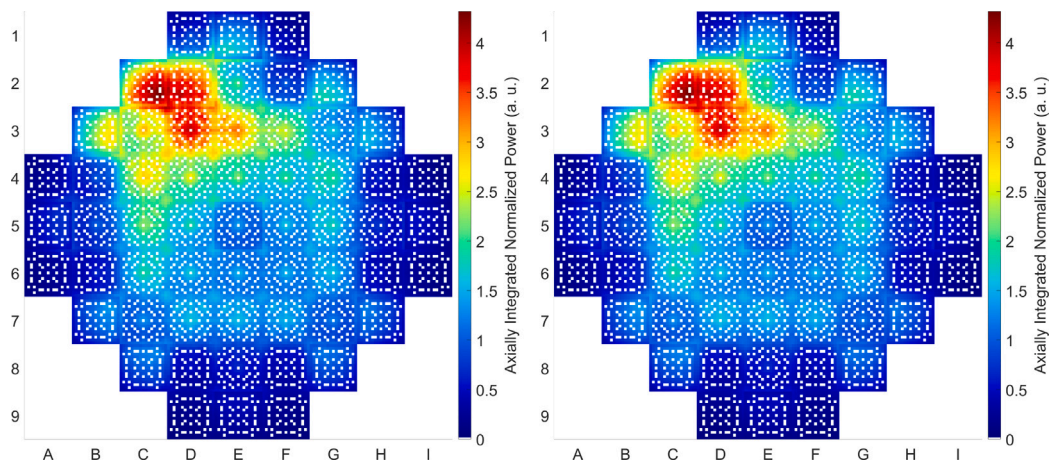

Fig. 5. Distribution of axially integrated normalised pin power at the time of maximum power (left: GUARDYAN-SCF, right: Serpent2-SCF).

which is a significant difference between the two Monte Carlo codes: Serpent2-SCF predicted a maximum value about 1.3 times the one of GUARDYAN-SCF. This difference has consequences on the thermal hydraulics properties as well, it appears that the temperatures usually start increasing simultaneously in Serpent2-SCF and GUARDYAN-SCF, but in the GUARDYAN-SCF simulations the peak values are lower. The peak power from the PARCS-SCF calculation is 48.35 times the nominal power, which is about 25% and 40% higher than the Serpent2-SCF and GUARDYAN-SCF results respectively.

The axially integrated power distributions of the Monte Carlo results at the time of the maximum are shown in Fig. 5. Although the maximum total power in the Serpent2-SCF calculation is notably higher, the pin level normalised power distribution of the two calculations is almost identical, the differences are below 2% on average. The fuel rod with the highest power according to the GUARDYAN-SCF and Serpent2-SCF calculation is located next to each other, C2-ROD(14,5) and C2-ROD(15,5) respectively.

The maximum fuel centerline temperature calculated by the different code systems are shown as a function of time in Fig. 6. The temperature calculated by GUARDYAN-SCF starts increasing at the same time as the Serpent2-SCF results, but reaches the maximum earlier, at 1.29 s compared to 1.53 s, and at a lower value as a consequence of lower peak power.

Although the maximum temperatures are different between the two Monte Carlo based solutions, the temperature maps at the time of the maximum presented in Fig. 7 are similar. The maximum centerline

temperature calculated by Serpent2-SCF was 1254.91 K observed in C2-ROD(13,4) at the 11th axial layer, while the maximum centerline temperature calculated using GUARDYAN-SCF was 1127.22 K located in C2-ROD(14,5) at the 16th axial layer.

Maximum coolant temperature evolutions are compared in Fig. 8, and the temperature maps at the time of the maximum, 1.128 s and 1.002 s for GUARDYAN-SCF and Serpent2-SCF respectively, are shown in Fig. 9. From Fig. 8 it can be assumed that in the Serpent2 simulation some coolant was boiling between 0.954 s and 1.32 s, where the temperature was about 615.3 K, the boiling point of water at 15 MPa.

The maximum coolant temperature according to the GUARDYAN-SCF calculation is 605.58 K at location C2-ROD(13,5), axial layer 30. The Serpent2-SCF calculation also predicts a maximum at this location.

Minimum departure from nucleate boiling ratio is well above 1 according to all code systems, 1.6177 using PARCS-SCF, 1.3032 from the Serpent2-SCF calculation, and 1.8538 from the GUARDYAN-SCF simulation. The minimum DNBR as a function of time can be seen in Fig. 10.

In Fig. 11 the DNBR map at the time of minimum can be seen. The minimum was in D2-ROD(1,1) according to both Monte Carlo codes at the 11th and 15th axial layer, 0.246 s and 0.288 s after the start of the transient using Serpent2-SCF and GUARDYAN-SCF respectively.

Overall, after the ejection of the control rod with the highest worth in a SMART-like SMR in BOC HZP conditions, for all three coupled code systems presented in this paper a power increase of 7 orders of magnitude was observed, but the temperature of the fuel and cladding was
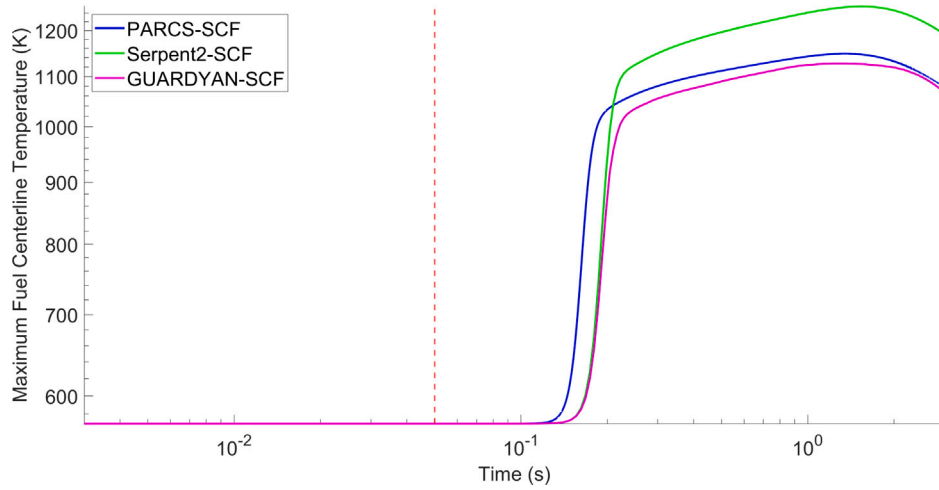
Fig. 6. Evolution of the maximum fuel centerline temperature during the transient starting from HZP as calculated by the three different code systems.
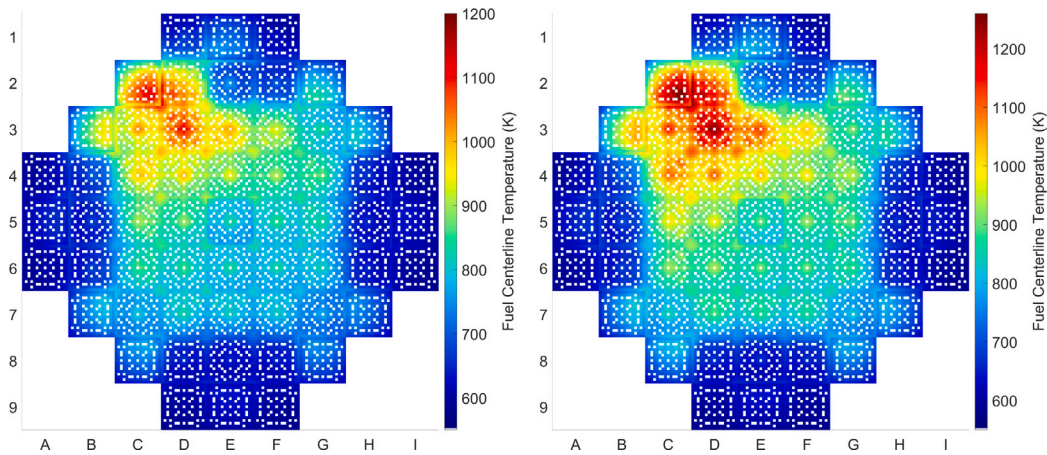

Fig. 7. Fuel centerline temperature map at the time and axial level of the maximum (left: GUARDYAN-SCF, right: Serpent2-SCF).
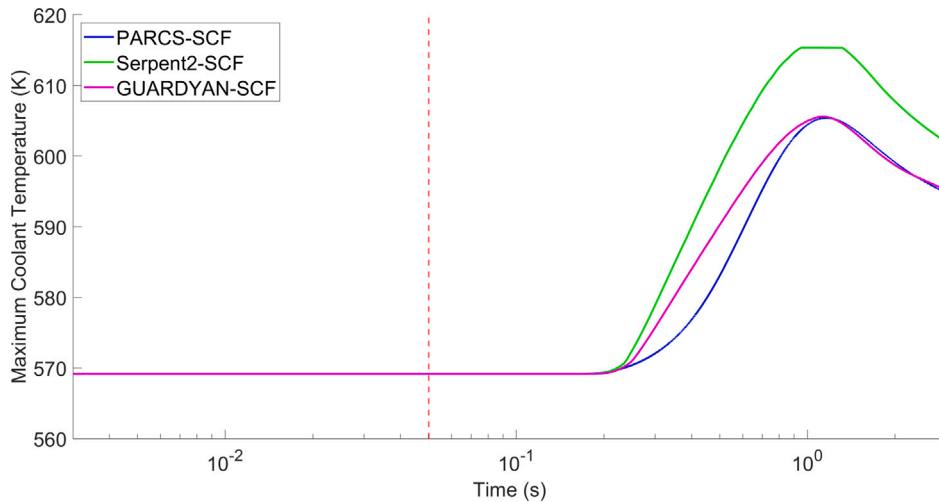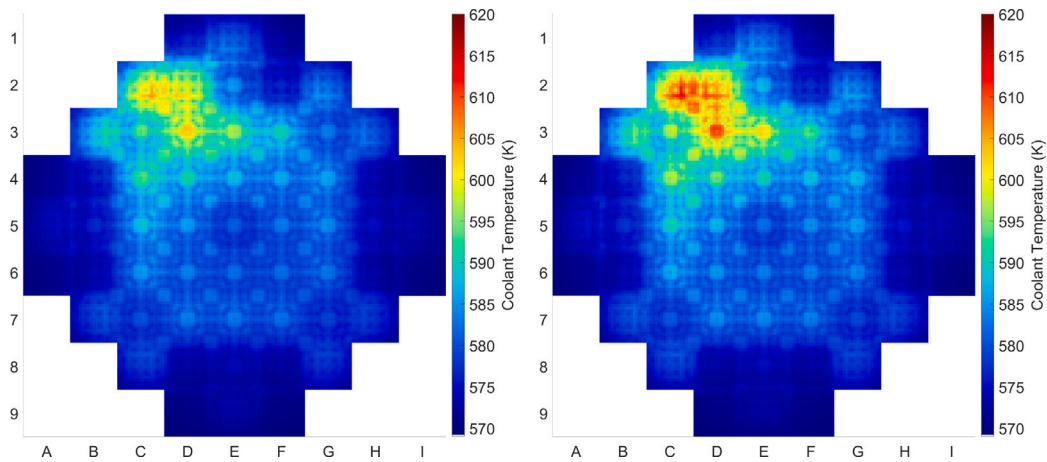

Fig. 8. Evolution of the maximum coolant temperature during the transient starting from HZP as calculated by the three different code systems.

well below their respective melting points during the whole transient. The DNBR was above 1, the lowest value was 1.3032 calculated using Serpent2-SCF. In the Serpent2-SCF simulation some coolant is likely boiling for about 0.4 s but this does not appear to have a noticeable negative effect on the heat removal from the fuel rods.

4.2. HFP results

In this section we will discuss the results of the simulation of a control rod ejection accident starting from BOC HFP conditions. Our GUARDYAN-SCF Monte Carlo based solutions will be presented, and

Fig. 9. Coolant temperature maps at the time and axial level of the maximum (left: GUARDYAN-SCF, right: Serpent2-SCF).
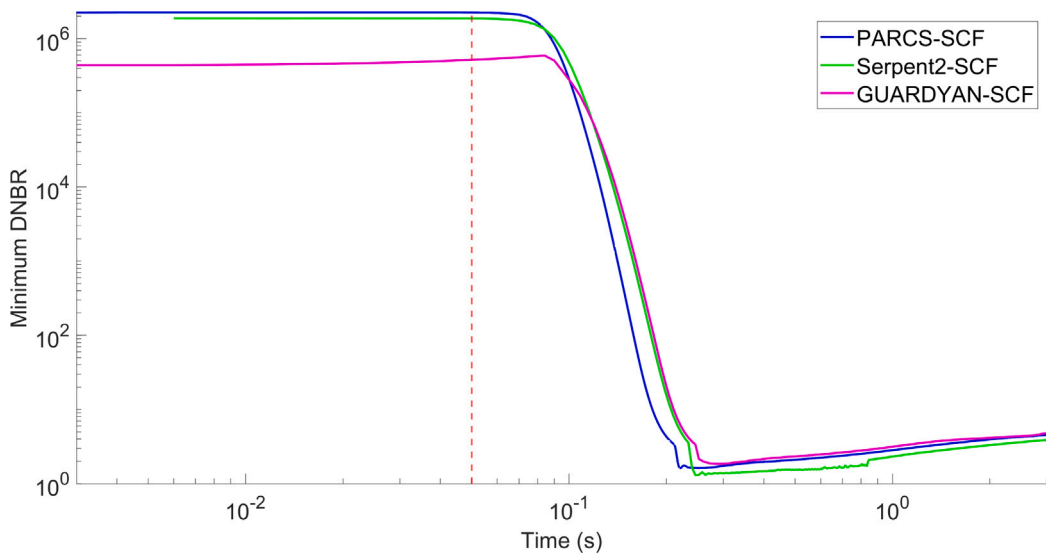
Fig. 10. Evolution of the minimum departure from nucleate boiling ratio during the transient starting from HZP as calculated by the three different code systems.
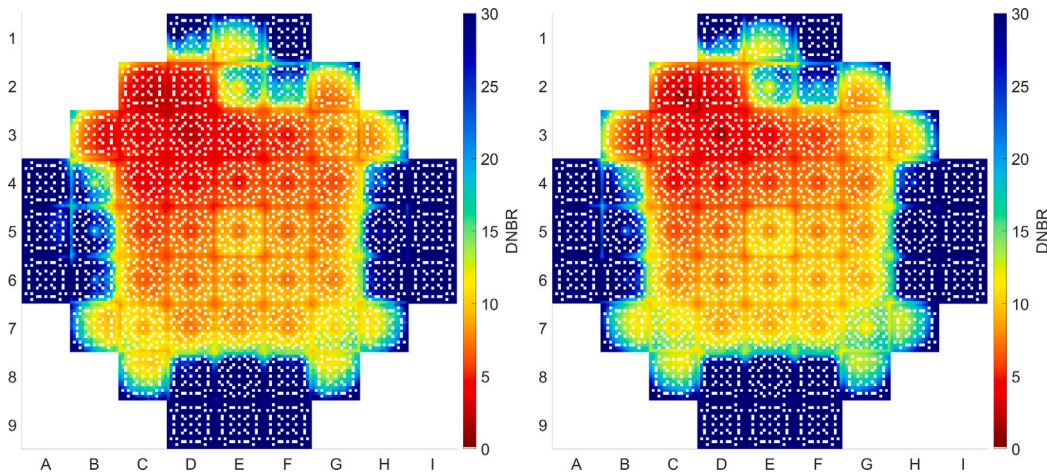
Fig. 11. Distribution of DNBR at the time and axial level of the minimum (left: GUARDYAN-SCF, right: Serpent2-SCF).

some peak values will be compared to deterministic PARCS-SCF results published in Alzaben et al. (2019a).

The total power of the reactor as a function of time is shown in Fig. 12. The peak power reached during the HFP case is 14.3 times the nominal power at 0.066 s, almost half of the maximum power of the HZP case. This effect is explained by the fact that as a consequence of the higher initial fuel temperature in the HFP case, the Doppler effect rapidly provided a large enough negative reactivity leading to a shorter
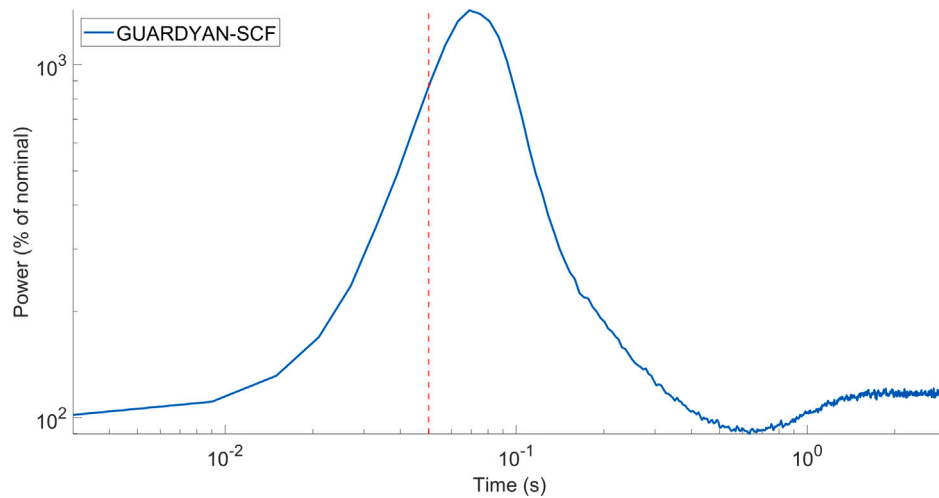
Fig. 12. Evolution of the total power during the HFP transient calculated by GUARDYAN-SCF.
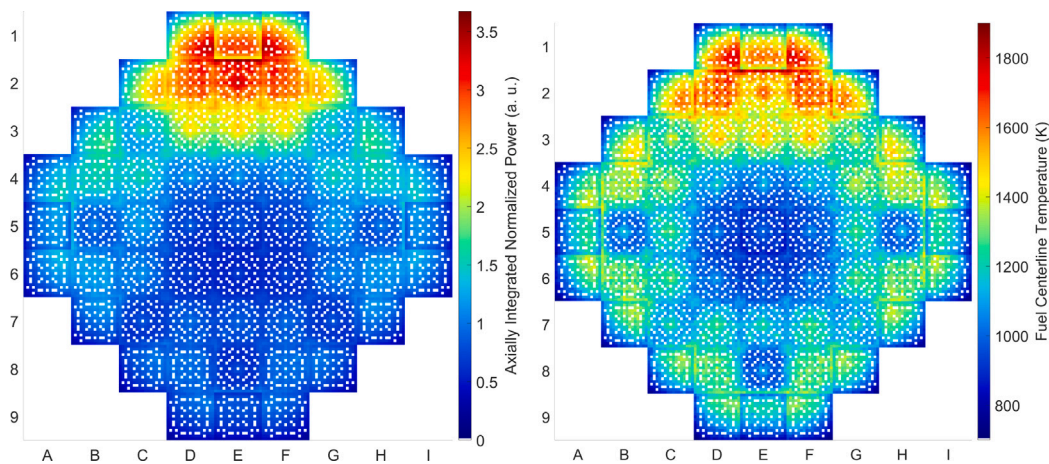
Fig. 13. Power distribution (left) and fuel centerline temperature (right) data calculated with GUARDYAN-SCF from HFP initial conditions.

power excursion with a significantly smaller maximum. The maximum predicted by the PARCS-SCF calculation was higher, at about 16 times the nominal power at 0.079 s.

The axially integrated normalised power distribution at the time of peak power can be seen in Fig. 13.

As it can be seen in Fig. 14, maximum fuel centerline temperature rises rapidly after the ejection, and after a period of increasing slower, it starts to rise faster again. This suggests that the heat removal from some fuel pins is insufficient. Looking at the average fuel centerline temperature, the graph shows a tendency similar to what we saw in the HZP case in Fig. 6. The maximum temperature was 1881.65 K observed at the 10th axial layer at 2.982 s, while during the PARCS-SCF calculation in Alzaben et al. (2019a) the maximum fuel centerline temperature reached about 1680 K. The fuel centerline map at the time and axial level of the maximum is shown in Fig. 13.

The evolution of the maximum coolant temperature is shown in Fig. 15. The maximum between 0.462 s and 0.858 s, and the plateau starting from 0.24 s until the end of the simulation means some moderator is boiling, thus heat removal is decreased which explains the continuous rise in maximum fuel centerline temperature, even as the average fuel centerline temperature starts to decrease. The PARCS-SCF calculations also show that the maximum coolant temperature reaches the saturation temperature, however it happens later, around 0.42 s.

The coolant temperature map at 0.462 s at the 30th axial layer is shown in Fig. 16 alongside a map of the core with the number of axial nodes with coolant temperature above 615 K (saturation temperature

at 15 MPa, i.e. nodes where moderator is boiling) is shown, and the same quantity was analysed at 0.24 s and 3 s to assess how the extent of boiling in the core is changing over the plateau seen in Fig. 15.

At 0.24 s moderator is boiling in 29 nodes in the top 30 cm of 10 fuel pins, this increased to 3307 nodes in the top third of 423 fuel rods at 0.462 s. At 3 s, the end of the simulation, the number of nodes with coolant temperature above 615 K is somewhat lower at 2868, although the number of fuel pins affected have increased to 580, located somewhat more tightly in the vicinity of the ejected CR.

The DNBR data against time is presented in Fig. 17, the minimum DNBR dips below 1 between 0.108 s and 0.36 s, then between 0.426 s and 0.63 s, with a minimum of 0.90548 at 0.138 s. At the time of the minimum, the DNBR is below 1 in 27 nodes, mostly around the upper corners of FA E2.

In Fig. 18 the DNBR map at the time of minimum is shown, as well as a close up of the upper part of the core with the number of axial nodes with DNBR under 1 marked. After the global minimum of the DNBR during the transient, values below 1 can be seen for about 0.5 s, thus we looked at how many nodes have DNB ratios below 1 at 0.534 s, the last local minimum of the DNBR, which turned out to be a single one. Node-wise DNBR values at the local minima 0.138 s and 0.534 s were arranged into histograms with 0.1 wide bins, and are partially shown in Fig. 19 to emphasise that the majority of nodes have values well above 1, most frequently around 2.5–3.

Overall it appears that during the transient starting from HFP the coolant starts to boil around some fuel rods and the DNBR is below 1
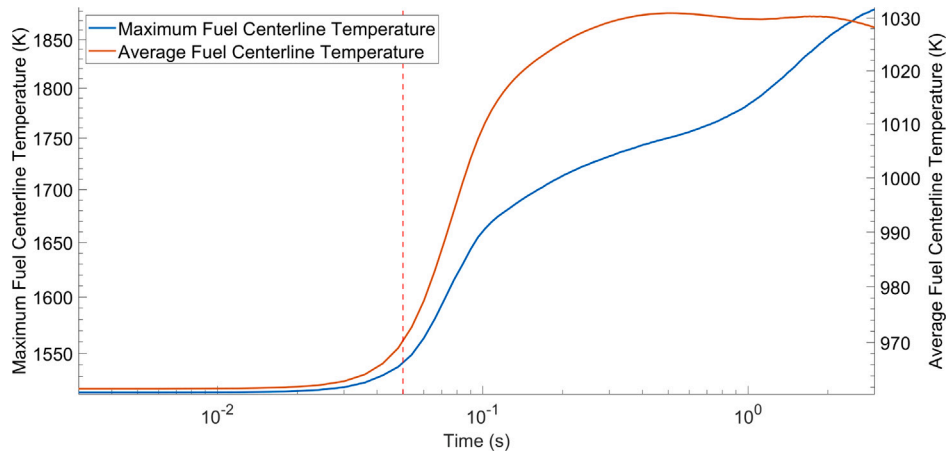
Fig. 14. Evolution of the maximum and average fuel centerline temperature during the HFP transient calculated by GUARDYAN-SCF.
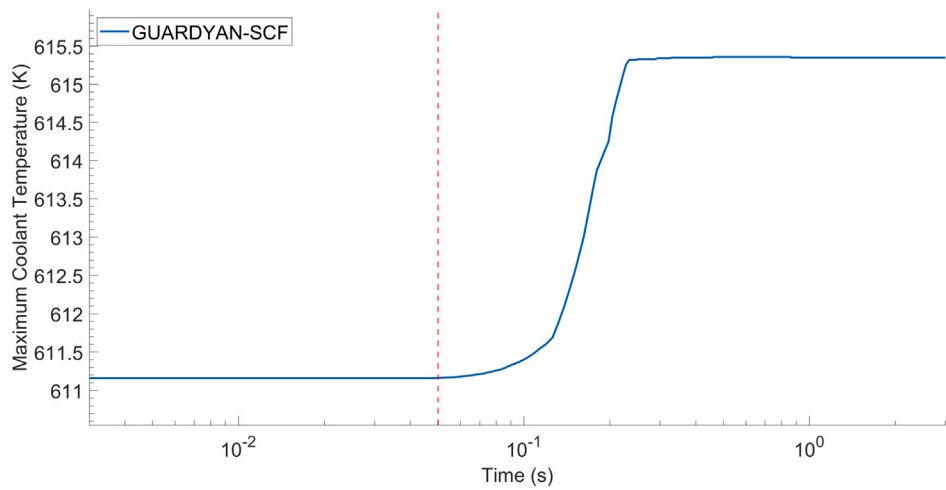

Fig. 15. Evolution of the maximum coolant temperature during the HFP transient calculated by GUARDYAN-SCF.
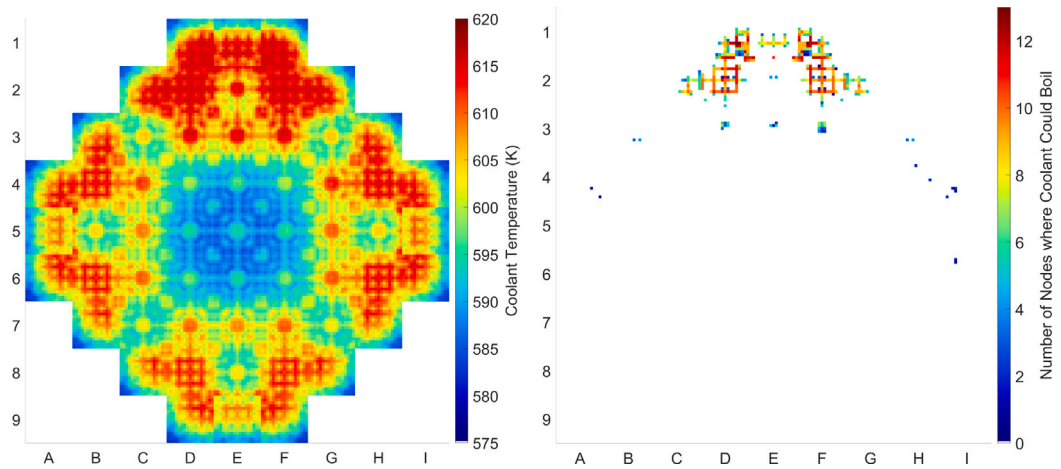

Fig. 16. Coolant temperature related data at 0.462 s.

at a few nodes for about 0.5 s. The DNBR increases well above 1 during the simulated 3 s of the transient, while the coolant temperature seems to slowly return to a temperature below the boiling point in most of the core. Although fuel and cladding temperatures are well below their melting points during the whole transient, a longer simulation could be advantageous to demonstrate moderator boiling remains at a safe level. The fact that DNBR values below 1 are present is somewhat concerning and further studies might be warranted by more experienced researchers in the field of reactor design and safety analysis. We must also note that in this section we presented data from a single realisation, and in the following section we will see that the DNBR calculated as the average of 8 realisations, even if slightly, stays above 1.
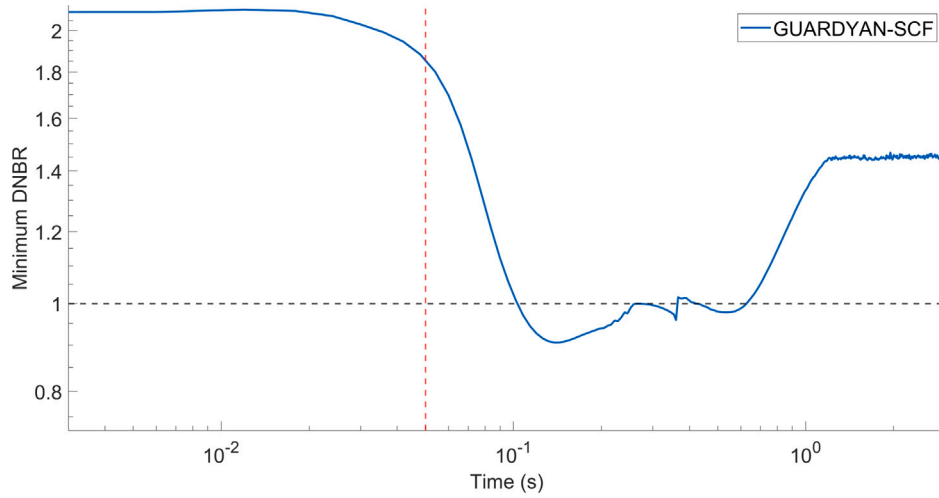
Fig. 17. Evolution of the minimum DNBR during the HFP transient calculated by GUARDYAN-SCF.
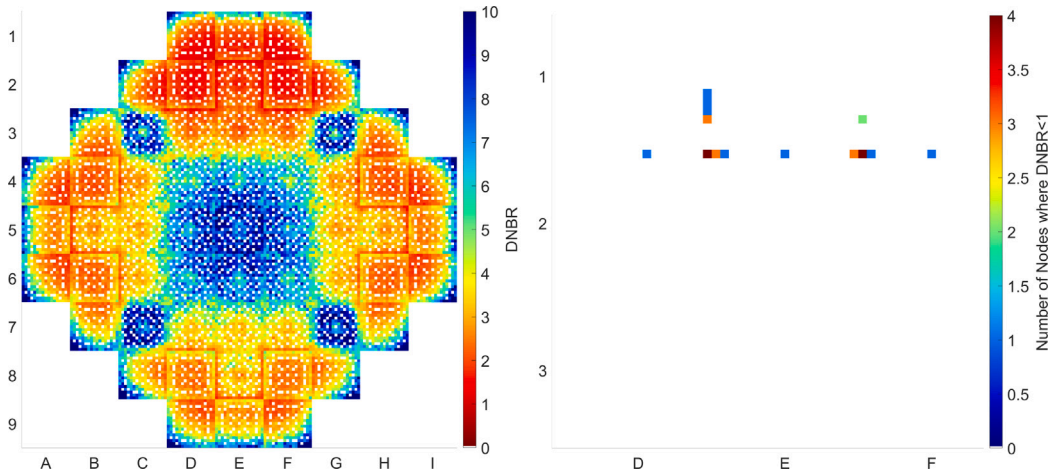

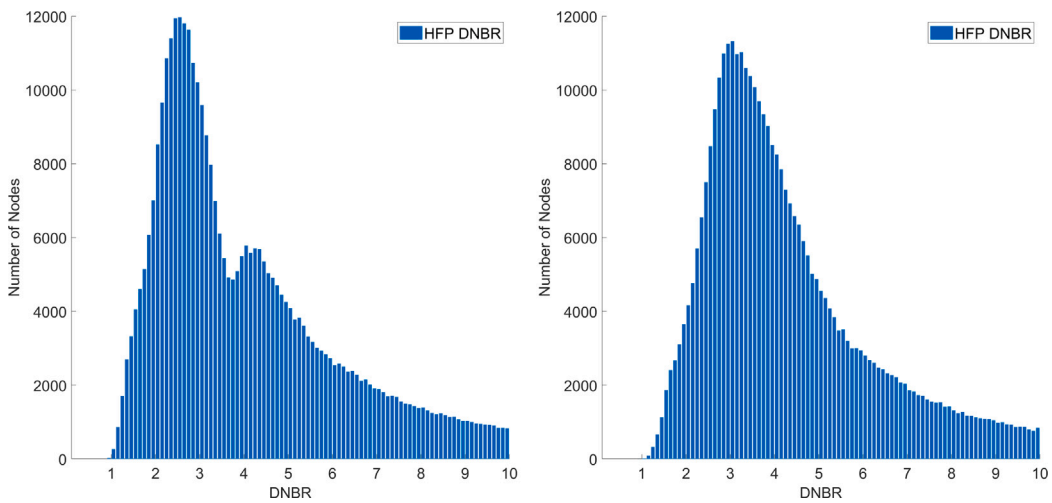**Fig. 18.** DNBR related data at 0.138 s.

Fig. 19. Histograms of node-wise DNBR values at local minima.

4.3. Variance analysis

When using Monte Carlo codes the variance of the results must be discussed. In order to have an estimation of the variance even with thermal hydraulic feedback, 8 simulations of the first 0.4 s of the transient were carried out with different random seeds for the congruential pseudorandom number generator used in GUARDYAN, both in HZP and HFP cases. From the realisations the relative variances
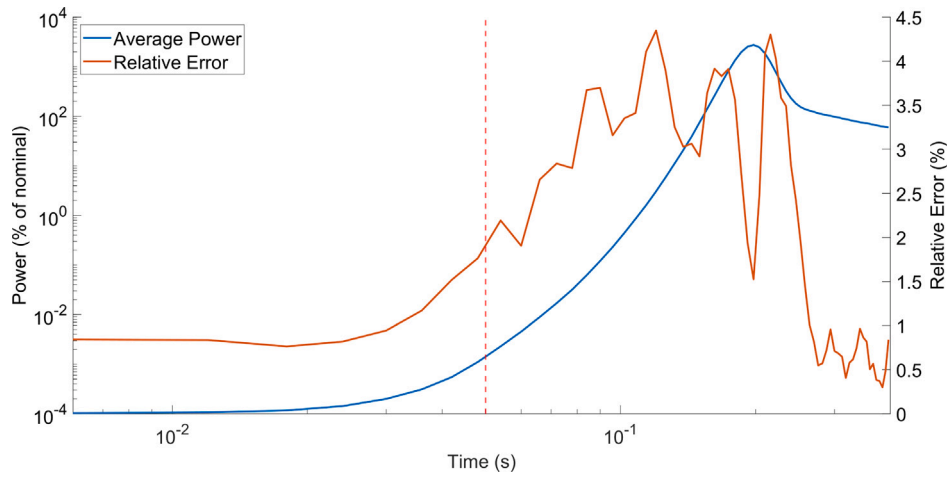
Fig. 20. Total power and the relative error of total power during the first 0.4 s of the HZP transient calculated from 8 GUARDYAN-SCF calculations with different random seeds.

Table 2
Relative variances of the studied quantities in the HZP cases: Δ_M is the relative variance of the maximum values, Δ_A is the relative variance of the average values.

	$T_{Fuel\ Centerline}$	$T_{Coolant}$	DNBR	$T_{Inner\ Cladding}$	$T_{Outer\ Cladding}$
$Avg(\Delta_M)$	0.197%	0.007%	1.396%	0.048%	0.013%
$Avg(\Delta_A)$	0.085%	0.001%	9.017%	0.018%	0.01%
$Max(\Delta_M)$	0.716%	0.025%	5.583%	0.166%	0.096%
$Max(\Delta_A)$	0.264%	0.005%	68.108%	0.036%	0.0213%

Table 3
Relative variances of the studied quantities in the HFP cases: Δ_M is the relative variance of the maximum values, Δ_A is the relative variance of the average values.

	$T_{Fuel\ Centerline}$	$T_{Coolant}$	DNBR	$T_{Inner\ Cladding}$	$T_{Outer\ Cladding}$
$Avg(\Delta_M)$	0.439%	0.005%	1.305%	0.127%	0.198%
$Avg(\Delta_A)$	0.089%	0.005%	9.57%	0.024%	0.007%
$Max(\Delta_M)$	0.615%	0.016%	1.958%	0.179%	0.378%
$Max(\Delta_A)$	0.121%	0.01%	68.916%	0.042%	0.009%

(expressed in percentages) were calculated according to Eq. (1), where c_i is the contribution of the ith of the N realisations to the quantity in question

$$\Delta\ (\%) = 100 \cdot \sqrt{\frac{\sum_{i=1}^{N} c_i^2}{\left(\sum_{i=1}^{N} c_i\right)^2} - \frac{1}{N}} \tag{1}$$

For the power data, the evolution of the variance of the total power was studied along with the variance of node wise power at the time of the peak power. For the thermal hydraulics quantities, the node wise variances were studied at certain times as well, along with the evolution of the variances of the maximum values over the core.

Relative variance along with the average total power is shown in Figs. 20 and 21 for the HZP and HFP cases respectively. The relative variance stayed below 4.5% during the whole 0.4 s in the HZP case and below 3% in the HFP case. Higher variances are observed when the total power itself changed rapidly, otherwise the values were around 1%, with the average being 2.006% in the HZP and 1.219% in the HFP case.

Node-wise variance of the power at the time of maximum in the HZP case was 3.7% on average with a maximum of 48.98%, and for the HFP case 3.4% on average with a 24.8% maximum. The node-wise maxima are located at the very first axial node, Average node-wise powers along the relative variance of node-wise power at the time and axial level of the maxima is shown in Figs. 22 and 23 for the HZP and HFP cases respectively.

For the variances of the temperatures and DNBR over time we considered both the maximum (and minimum in the case of DNBR) values in the core, as well as the values averaged over the core. The average and maximum relative variances are summarised in Tables 2 and 3 for the HZP and HFP cases respectively.

Variances of the average temperatures usually increased when the temperatures were changing. The exceptions are the coolant temperature, the variance of which continuously increased, but was also very low to begin with, and the DNBR that had some large fluctuations in the first half of the simulation, where the DNBR values were large.

As an example, in Figs. 24 and 25 the evolution of the average fuel centerline temperature with the relative variance is shown for the HZP and HFP cases respectively. Concerning the variances of the average DNBR values, the maxima of almost 70% are located at times when the DNBR itself is so high that even if it was lower by 99% the value would be in the 10^6 range.

For the DNB ratios the minimum is in the first 0.4 s of the transient in both HZP and HFP cases, as is the beginning of the plateau of the coolant temperature in the HFP case, thus the node-wise relative variance of these three quantities were studied at these times. From the average of the 8 realisations these times are 0.3 s and 0.156 s for the minimum DNBR in the HZP and HFP cases respectively, and 0.384 s for the maximum coolant temperature in the HFP case.

Fig. 26 shows the average coolant temperature and the relative variance of the coolant temperature at the time and axial level of the maximum. Higher variances are mostly around the ejected control rod, where the coolant temperature itself is higher, but even these higher variances are low, 0.046% at most and 0.012% on average.

DNBR maps along their relative variance at the time of the minimum are shown in Figs. 27 and 28 for the HZP and HFP cases. The minimum of the average DNBR is above 1 in both HZP and HFP cases, 1.8999 and 1.056 respectively. The relative variance of the DNBR in the HZP case was at maximum 21.402% and 1.376% on average, while in the HFP case the maximum was 30.76% with an average of 2.706%. The maxima were located at the bottom of the active core in both cases.

Overall the node-wise variance of the results are satisfactory, for the power and DNBR, histograms of the relative variance with 0.1% wide bins at the time of maximum in HZP and HFP cases are shown in Fig. 29. Generally the HZP results have slightly lower relative variances and even in the HFP case the variances are in the few percent range. The maxima of the node-wise relative variances were observed at the edge of the core, which is were generally less particles and thus suboptimal statistics are expected.
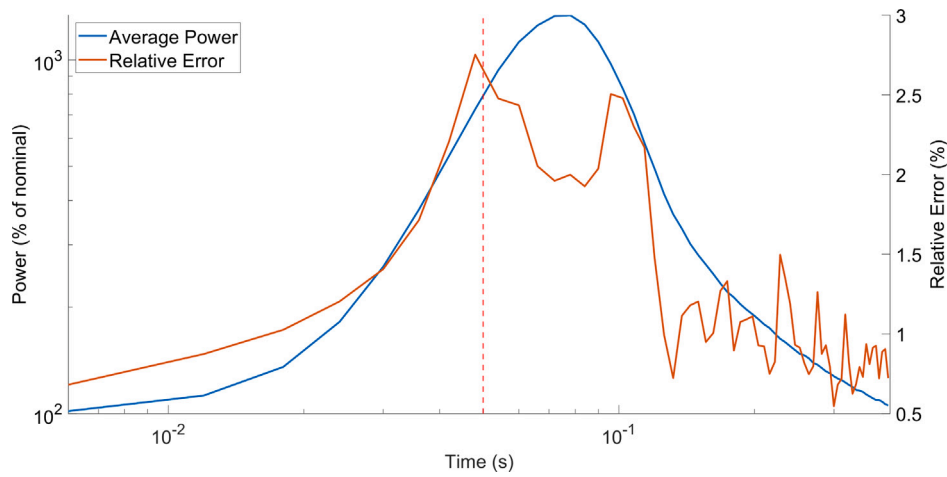
Fig. 21. Total power and the relative error of total power during the first 0.4 s of the HFP transient calculated from 8 GUARDYAN-SCF calculations with different random seeds.
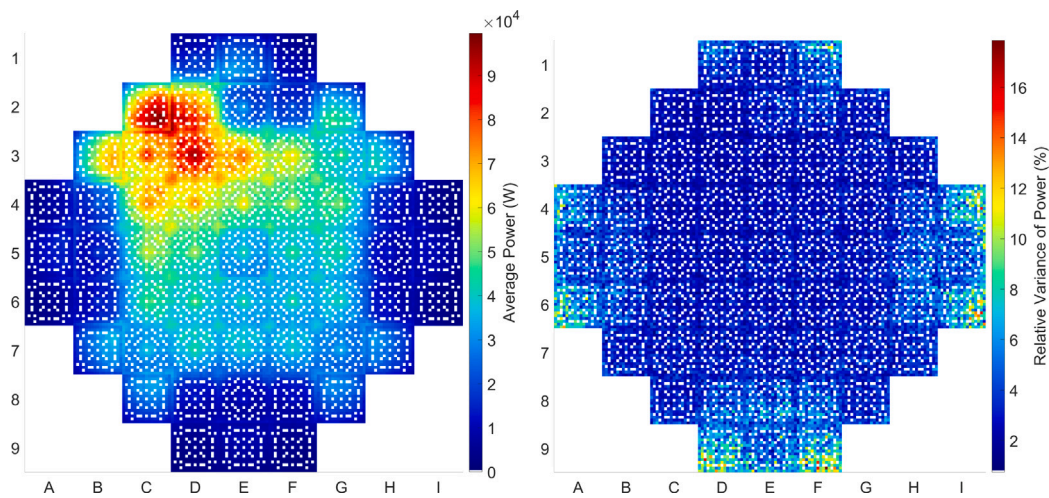

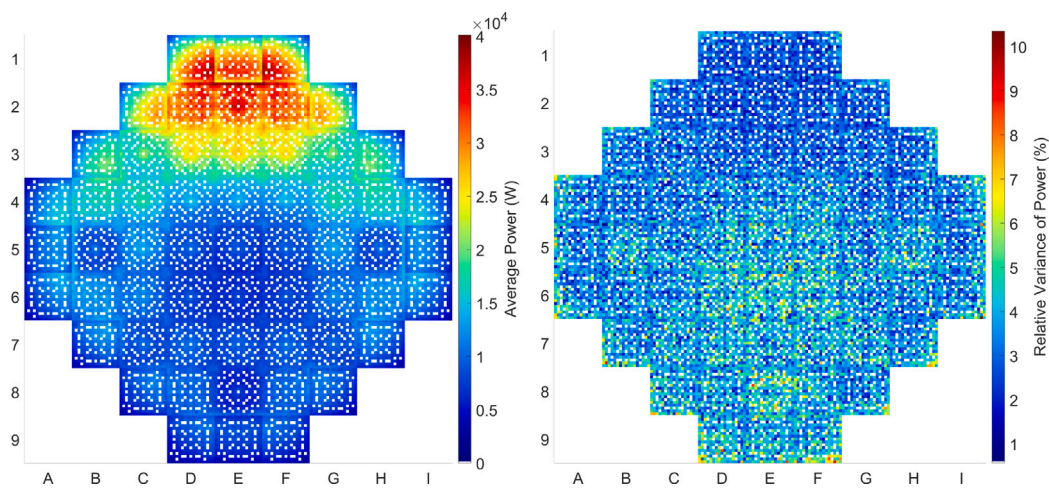**Fig. 22.** Node-wise power data at 0.192 s, 13th axial layer in the HZP case.

Fig. 23. Node-wise power data at 0.0072 s, 10th axial layer in the HFP case.

5. Conclusion

We used the GUARDYAN GPU based dynamic Monte Carlo neutronics code coupled with the SUBCHANFLOW subchannel thermal hydraulics code to model the ejection of the control rod with the highest worth in a SMART-like SMR model, starting from BOC HZP and HFP conditions. The HZP results were compared to PARCS-SCF nodal based deterministic and Serpent2-SCF pin-by-pin Monte Carlo
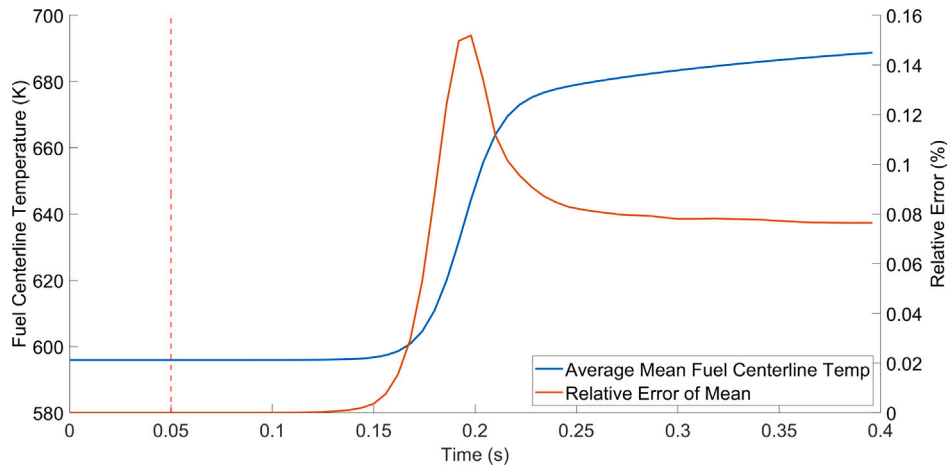
Fig. 24. Mean fuel centerline temperature and the relative error of mean fuel centerline temperature during the first 0.4 s of the HZP transient calculated from 8 GUARDYAN-SCF calculations with different random seeds.
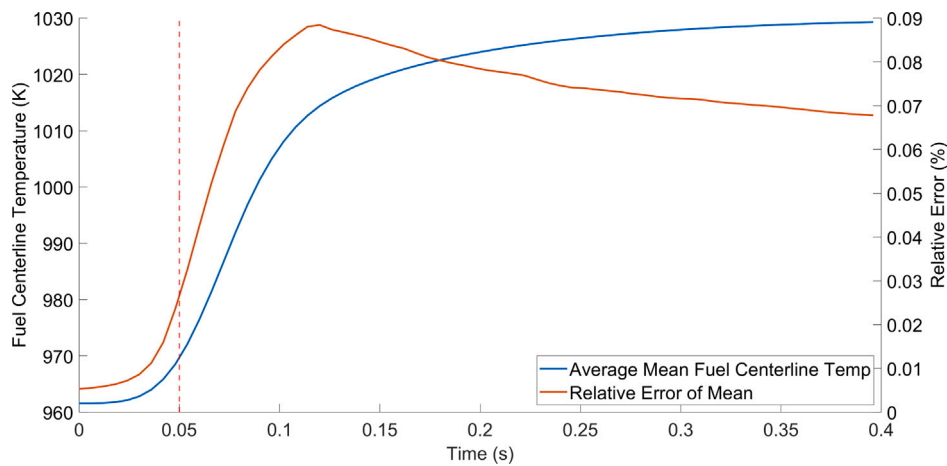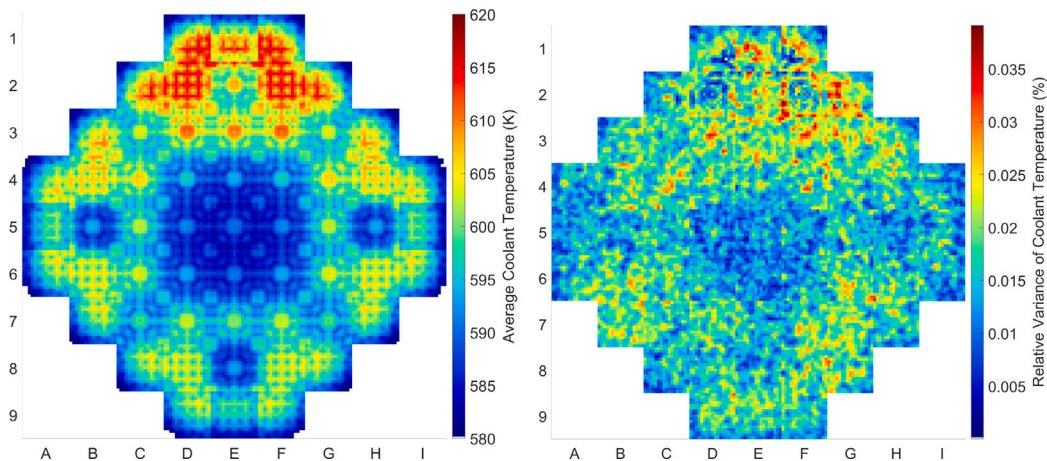

Fig. 25. Mean fuel centerline temperature and the relative error of mean fuel centerline temperature during the first 0.4 s of the HFP transient calculated from 8 GUARDYAN-SCF calculations with different random seeds.

Fig. 26. Node-wise coolant temperature data at 0.384 s, 21st axial layer in the HFP case.

based solutions. The time evolution of the power and the thermal hydraulic properties calculated using GUARDYAN-SCF showed a similar behaviour as the ones calculated using Serpent2-SCF, with lower maximum values. This difference between the two Monte Carlo based solutions is likely due to the different coupling timesteps. In the HZP case, all of the materials used in the fuel rods stayed well below their

respective melting points during the whole transient, the minimum DNBR was above 1.3 in all cases, and the maximum coolant temperature of the Serpent2 calculation suggests that some moderator is boiling. The two Monte Carlo based calculations gave similar results, and their applicability in our opinion depends highly on the resources available to the user: the Serpent2-SCF calculations were running faster
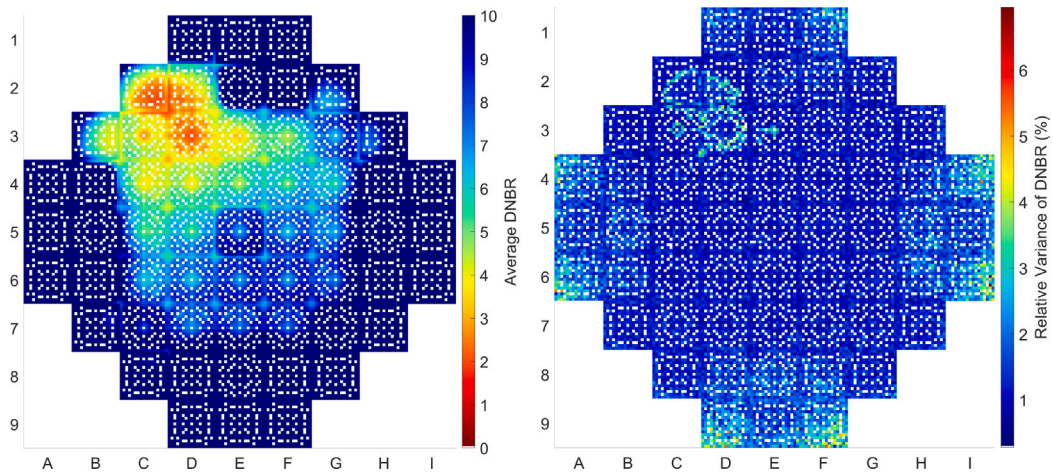
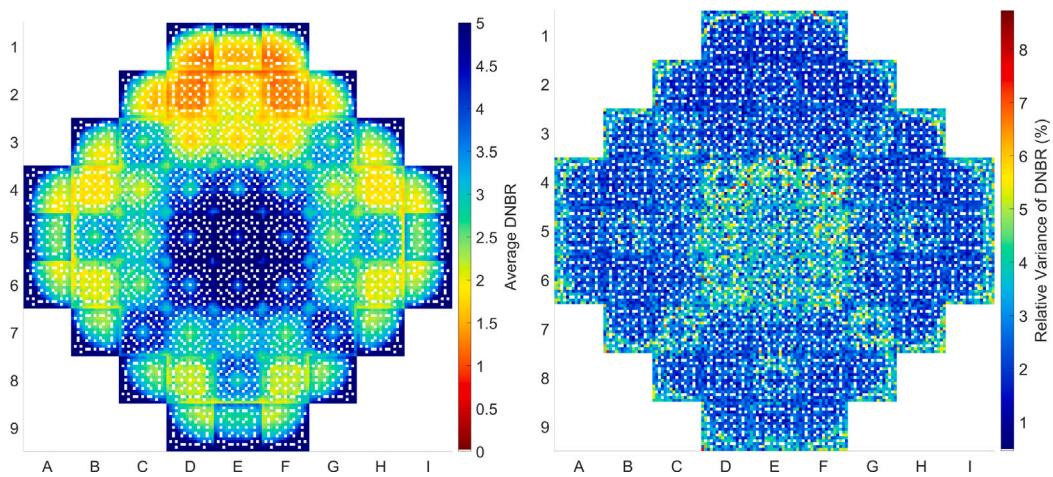**Fig. 27.** Node-wise DNBR data at 0.3 s, 15th axial layer in the HZP case.

Fig. 28. Node-wise DNBR data at 0.156 s, 22nd axial layer in the HFP case.
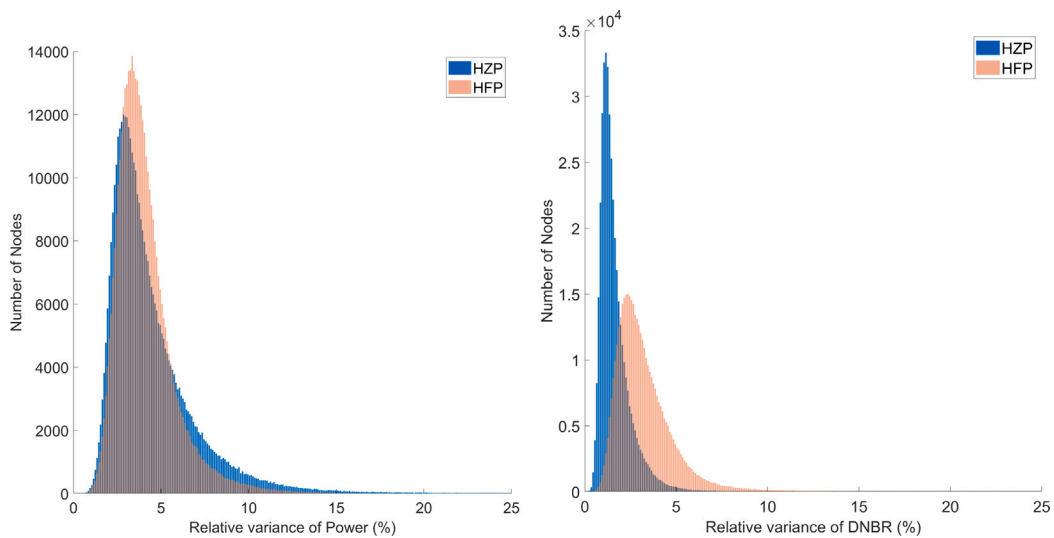

Fig. 29. Histograms of node-wise relative variances of power and DNBR at the time of maxima.

on a proper CPU cluster, while the GUARDYAN-SCF calculations took significantly longer, but used hardware comparable to a slightly above average home computer without restriction to utilise GPU clusters as well.

The HFP results were similar to PARCS-SCF calculations published in Alzaben et al. (2019a). During the HFP transient the power increase stopped in about a third of the time necessary in the HZP case, and the maximum power was about half of that of the HZP peak. Based

on the maximum coolant temperature, moderator was boiling around some fuel rods for about 2.75 s, and the minimum DNBR was below 1 for about 0.5 s. The DNBR increased above 1 before the end of the simulated 3 s of the transient, and affected at most 0.0055% of the nodes. The number of nodes where coolant temperature was above the boiling point decreased between the time of maximum coolant temperature and the end of the simulation, but boiling could still be assumed in 2868 nodes of 580 fuel rods, thus a longer simulation might be useful in order to make sure boiling stops and maximum fuel centerline temperature decreases as well.

Declaration of competing interest

The authors declare that they have no known competing financial interests or personal relationships that could have appeared to influence the work reported in this paper.

Acknowledgements

Data availability

Data will be made available on request.

References

Alzaben, Y., Sanchez-Espinoza, V.H., Stieglitz, R., 2019a. Analysis of a control rod ejection accident in a boron-free small modular reactor with coupled neutronics/thermal-hydraulics code. Ann. Nucl. Energy 134, 114–124. http://dx.doi.org/10.1016/j.anucene.2019.06.009.

Alzaben, Y., Sanchez-Espinoza, V.H., Stieglitz, R., 2019b. Core neutronics and safety characteristics of a boron-free core for small modular reactors. Ann. Nucl. Energy 132, 70–81. http://dx.doi.org/10.1016/j.anucene.2019.04.017.

Basualdo, J.R., Sanchez-Espinoza, V., Stieglitz, R., Macian-Juan, R., 2020. Integration of the subchannel thermal-hydraulic code SubChanFlow into the reactor dynamics code PARCS: Development and testing based on a computational benchmark. Prog. Nucl. Energy 119, http://dx.doi.org/10.1016/j.pnucene.2019.103138.

Boroczki, Z.I., Klujber, G., Tolnai, G., Molnar, B., Legrady, D., Gabrielli, F., Rineiski, A., Szieberth, M., 2020. Simulation of a research reactor reactivity transient with deterministic and GPU-assisted Monte Carlo reactor kinetics codes. Eur. Phys. J. Plus 135 (3), http://dx.doi.org/10.1140/epjp/s13360-020-00280-4.

Downar, T., 2017. PARCS V3.3.0 - Volume I: Input Manual. Nuclear Engineering and Radiological Sciences. University of Michigan, s.l. Ann Arbor, MI, USA.

Ferraro, D., García, M., Valtavirta, V., Imke, U., Tuominen, R., Leppänen, J., Sanchez-Espinoza, V., 2020. Serpent/SUBCHANFLOW pin-by-pin coupled transient calculations for a PWR minicore. Ann. Nucl. Energy 137, http://dx.doi.org/10.1016/j.anucene.2020.107387.

Garcia, M., Tuominen, R., Gomlich, A., Ferraro, D., Valtavirta, V., Imke, U., van Uffelen, P., Mercatali, L., Sanchez-Espinoza, V.H., Leppäanen, J., Kliem, S., 2019. A Serpent2-subchanflow-transuranus coupling for pin-by-pin depletion calculations in light water reactors. Ann. Nucl. Energy 139, http://dx.doi.org/10.1016/j.anucene.2019.107213.

Imke, U., Sanchez, V.H., 2012. Validation of the subchannel code subchanflow using the NUPEC PWR tests (PSBT). Sci. Technol. Nucl. Install. 12, 1–12. http://dx.doi.org/10.1155/2012/465059.

Legrady, D., Halasz, M., Kophazi, J., Molnar, B., Tolnai, G., 2020. Population-based variance reduction for dynamic Monte Carlo. Ann. Nucl. Energy 149, http://dx.doi.org/10.1016/j.anucene.2020.107752.

Legrady, D., Hoogenboom, J.E., 2008. Scouting the feasibility of Monte Carlo reactor dynamics simulations. In: Proceedings of the International Conference on the Physics of Reactors 2008. PHYSOR08, Paul Scherrer Institut, Interlaken, Switzerland.

Legrady, D., Pukler, M., Panka, B., Tolnai, G., 2023. Coupling the GUARDYAN code to subchanflow. EPJ Nucl. Sci. Technol. 9 (11), http://dx.doi.org/10.1051/epjn/2023002.

Legrady, D., Tolnai, G., Hajas, T., Pazman, E., Parko, T., Pos, I., 2022. Full core pin-level VVER-440 simulation of a rod drop experiment with the GPU-based Monte Carlo code GUARDYAN. Energies 15 (2712), http://dx.doi.org/10.3390/en15082712.

Leppänen, J., Pusa, M., Viitanen, T., Valtavirta, V., Kaltiaisenaho, T., 2015. The serpent Monte Carlo code: Status, development and applications in 2013. Ann. Nucl. Energy 82, 142–150. http://dx.doi.org/10.1016/j.anucene.2014.08.024.

Mercatali, L., Huaccho, G., Sanchez-Espinoza, V.H., 2023. Multiphysics modeling of a reactivity insertion transient at different fidelity levels in support to the safety assessment of a SMART-like small modular reactor. Front. Energy Res. 11, 1130554. http://dx.doi.org/10.3389/fenrg.2023.1130554.

Molnar, B., Tolnai, G., Legrady, D., 2019. A GPU-based direct Monte Carlo simulation of time dependence in nuclear reactors. Ann. Nucl. Energy 132, 46–63. http://dx.doi.org/10.1016/j.anucene.2019.03.024.

Sanchez-Espinoza, V.H., Mercatali, L., Leppänen, J., Hoogenboom, E., Vocka, R., Dufek, J., 2021. The McSAFE project - high-performance Monte Carlo based methods for safety demonstration: From proof of concept to industry applications. EPJ Web Conf. 247, http://dx.doi.org/10.1051/epjconf/202124706004.

Sjenitzer, B.L., Hoogenboom, J.E., 2013. Dynamic Monte Carlo method for nuclear reactor kinetics calculations. Nucl. Sci. Eng. 175, 94–107. http://dx.doi.org/10.13182/NSE12-44.